Development of a Pilot Model of Hypersonic Rarefied Wind-Tunnel

Kazuhisa FUJITA, Toshiyuki SUZUKI and Takashi OZAWA

Aerospace Research & Development Directorate, JAXA, Chofu, Tokyo, 182-8522 JAPAN

Abstract. A pilot model of the hypersonic rarefied wind-tunnel (HRWT) has been developed and its flow characteristics have been measured. The HRWT consists of a gas heater which produces an increase in working gas temperature, an expansion nozzle with a large expansion ratio, a vacuum chamber as the test section, and an evacuation system with high exhaust velocity to allow a continuous operation at low ambient pressures. The nozzle exit diameter is 100 mm, which enables a quasi-uniform core flow diameter of 10 mm with Knudsen numbers at the order of 0.1 cm^{-1}. The flow characteristics in the test section have been measured with the aid of direct-simulation Monte-Carlo calculations of rarefied flows around the test model.

Keywords: Rarefied wind tunnel, Transition flow, Rarefied aerodynamics, DSMC

INTRODUCTION

The aerodynamic performance of aerospace vehicles in the hypersonic rarefied flight regime is of considerable interest for development of atmospheric reentry systems, planetary entry probes, and super low-altitude satellites[1], since the aerodynamic characteristics of the vehicle in rarefied flows considerably differ from those in dense and continuum flows. For example, it is known that the aerodynamic center of atmospheric reentry capsules moves more quickly in rarefied flows along with the angle of attack, resulting in a reduction of both static and dynamic stability about pitching motion compared to that in continuum flows[2].

In general, the rarefied aerodynamic performance for such vehicles in hypersonic free-molecular and transition flows is estimated by direct simulation Monte-Carlo (DSMC) calculations of the flow around the vehicle, since it is difficult and costly to realize the rarefied hypersonic test flow equivalent to the flight environments in ground test facilities. State-of-the-art techniques for DSMC simulation are highly sophisticated enough to offer useful information of the rarefied aerodynamics[3, 4]. However, there still remain considerable demands of direct measurement of the vehicle aerodynamics and the heat transfer rate in hypersonic rarefied flows, since it is often difficult to verify DSMC predictions by experiments. In addition, the numerical simulation often suffers from inevitable uncertainties originating from the accommodation factor of molecules colliding against the vehicle surface, which is difficult to exactly determine without experiments. Historically, a lot of experimentations have been conducted for rarefied gas research[5, 6, 7, 8, 9, 10]. Following these studies, in an attempt to offer the ground test environments of rarefied flows with high quality, a pilot model of the hypersonic rarefied wind tunnel (HRWT) has been developed in this study at Aerospace Research Center in Japan Aerospace Exploration Agency.

EXPERIMENTAL APPARATUS

A schematic view of the HRWT is shown in Fig.1. To design the HRWT of moderate dimensions, the computational fluid dynamic (CFD) and DSMC analyses were conducted. The numerical results have shown that, in order to increase the diameter of the core flow where the radial distribution of flow properties can be regarded to be uniform, the nozzle half-cone angle should be increased from that optimized for general hypersonic wind-tunnels. This is because thickness of the boundary layer increases as the flow becomes rarefied. Above all, a conical nozzle with a 20-deg half-cone angle was found to be the most suitable for the HRWT under consideration. It was also found that the evacuation system should have a high exhaust capacity to maintain the ambient static pressure low enough to avoid under expansion. From these analyses, the evacuation system is designed to consist of three turbo molecular pumps, ULVAC UTM-3303FH, each of which has a 3300 l/min exhaust capacity, and a back-up pump, ULVAC LR300, which has a 6,000 l/min exhaust capacity. The vacuum chamber is 1.0 m in diameter and 1.5 m in length. The expansion nozzle is designed to be 1.63 mm in throat diameter and 100 mm in exit diameter, having a 20-deg half-cone angle.

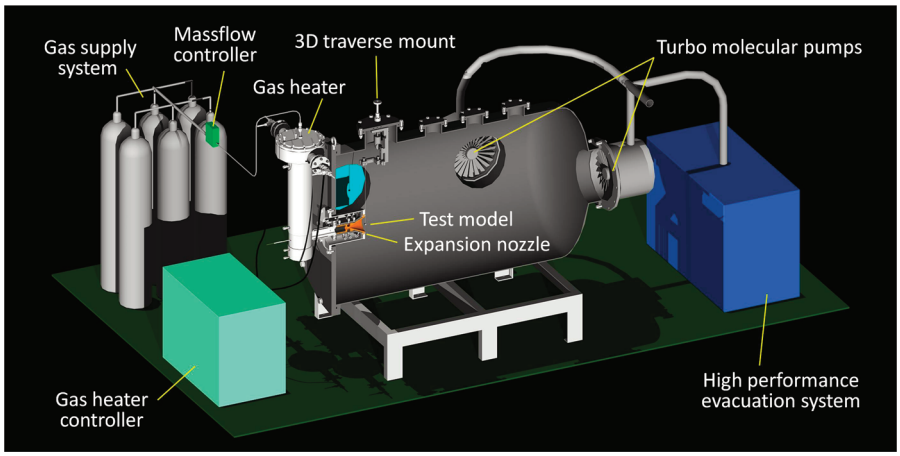

FIGURE 1. Schematic view of hypersonic rarefied wind tunnel (HRWT).

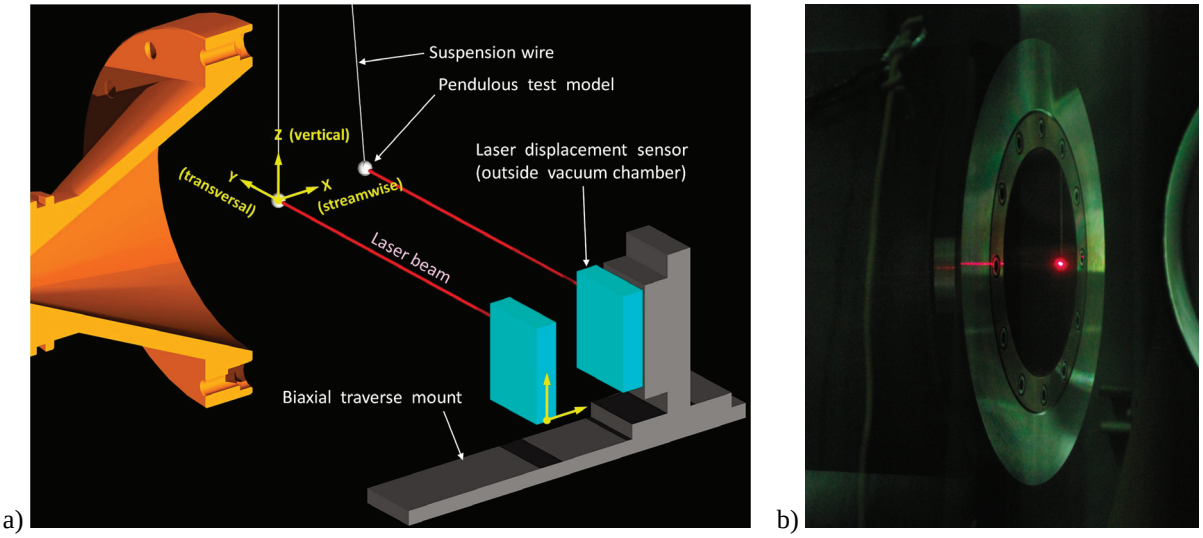

FIGURE 2. Displacement measurement system; a) schematic view and b) laser spot on test model.

Using the above system, the core diameter of the test flow as large as 10 mm is expected at $M = 10$ with the nitrogen flow rate of 0.03 g/s. At this design point, the static pressure at the test section is expected to be below 0.3 Pa, which yields the Knudsen number at the order of 0.1 cm $^{-1}$.

A test gas supplied from a gas supply system is first heated by an electric gas heater up to 1,800 K to increase the Mach number and the static temperature of flows in the test section. To avoid contaminations from the test flow, a dischargeless heating system is selected. The electric gas heater consists of a tungsten mesh heater, two layers of thermal insulators made of zirconia (inner layer) and alumina (outer layer) which cover the tungsten mesh heater, and a water-cooled outer structure made of stainless steel. In order to avoid oxidation of the tungsten mesh heater at high temperatures (up to 2,100 K), inert gases such as pure nitrogen and noble gases with purity higher than 99.999% are only allowed for use as the working gas. The electric gas heater can operated at 40 kW for the nitrogen mass flow rate of 0.1 g/s. Unfortunately, at this moment, the electric power supply system for the heater is still under preliminary operation tests. For this reason, the results of flow measurements as well as numerical simulations for cold flows are only presented in this article.

The aerodynamic forces acting on the test model are deduced from displacement of the pendulous model exposed in the test flow, as shown in Fig.2a. In order to measure the radial distribution of flow properties, a stainless-steel sphere model having a 5.00 ± 0.01-mm diameter is used in this study. The model is suspended by a stainless-steel wire having

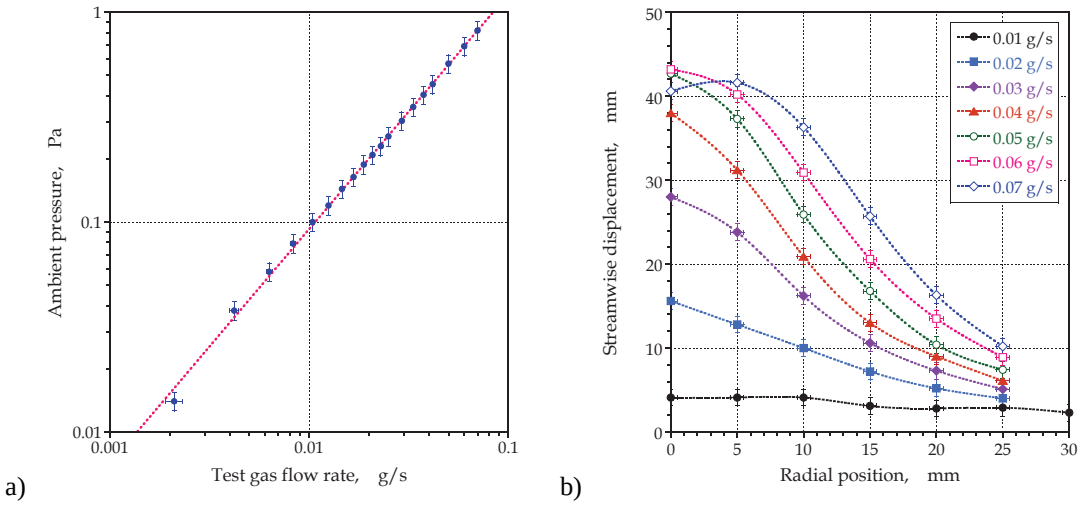

FIGURE 3. Experimental results; a) ambient pressure and b) variation of model displacement with radial position.

a 0.02 ± 0.002 diameter. The wire is connected to a traverse mount which allows triaxial adjustment of the test model position in relation to the test flow. To calibrate the force measurement procedure, influences of the wire were assessed. It is found that, in the flow conditions under consideration, the flexural rigidity of the wire and the aerodynamic force acting on the wire are small enough to be neglected in comparison to the aerodynamic force acting on the model.

The displacement of the test model was measured by a long-range laser displacement sensor, KEYENCE LK-G505. The displacement sensor was mounted on a high-accuracy biaxial traverse mount so that the laser can catch up with the model displacement both in the streamwise (x) and the vertical (z) direction (see Fig.2b). The streamwise and the vertical displacement of the test model were deduced from the shift of the displacement sensor in the corresponding directions from the original position, while the transversal (y) displacement was determined from the output signal of the displacement sensor. In general, the transversal displacement was seen to be less than 0.1 mm, suggesting the axisymmetric flow downstream the nozzle exit. Errors in model displacement measurement are expected to be ± 1.0 mm in the streamwise direction, and ± 0.5 mm in the vertical direction. Such considerable errors are due to inaccuracy in manually targeting the laser at the center of the test model. We are currently attempting to improve accuracy in model displacement measurement by introducing image processing technique using CCD cameras.

EXPERIMENTAL RESULTS

The HRWT was operated by changing the nitrogen flow rate up to 0.1 g/s. The ambient pressure, which is measured 1.0 m downstream of the nozzle exit, is shown in Fig.3a. It is seen that the ambient pressure increases exponentially with the flow rate, as indicated by a dotted line, and is maintained below 0.3 Pa at the flow rate of 0.03 g/s as designed. To measure radial distribution of flow properties, the sphere test model was located at 10-mm downstream positions from the nozzle exit by changing radial distance from the flow center. The results are shown in Fig.3b. It is seen that a significant radial change exists in the outer region of the test flow. As the flow rate increases, the radial change is suppressed around the flow center. It should be noted that the test model has a diameter of 5.00 mm so that the displacement only represents the average dynamic pressure about the model center with a spatial resolution lower than ± 2.5.

NUMERICAL ANALYSIS

Since the experimental results offer only limited information of the test flow, numerical simulations are conducted below to obtain more detailed knowledge of the flow properties in the test section. Once the model displacement observed in the experiment is reproduced by a coupled simulation of the flow with model motion, the flow properties are expected to be deduced from the computed flow field. In this study, the nozzle flow was calculated using a DSMC

TABLE 1. Knudsen number and flow properties at nozzle exit

$\dot{m}$, g/s	p_0, Pa	v_e, m/s	T_e, K	M_e	K_n ($L = 5$ mm)
0.01	2,650	704.3	56.7	4.6	1.02
0.02	5,000	729.8	22.3	7.6	0.165
0.03	7,325	735.9	14.5	9.5	0.082

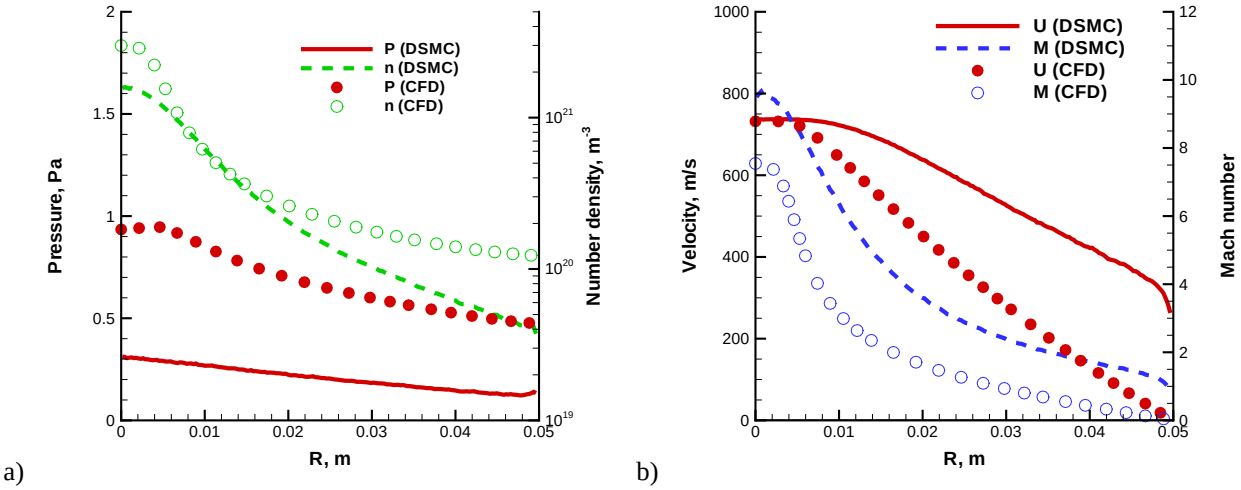

FIGURE 4. Comparison of pressure, number density, streamwise velocity, and Mach number between CFD (symbols) and DSMC (lines) at nozzle exit for $\dot{m} = 0.03$ g/s.

code, MOTIF (modeling of transitional-ionized flows), which has been developed to simulate rarefied nozzle flows and planetary atmospheric entry flows[11].

In Table 1, the flow properties computed by the DSMC method at the nozzle exit on the symmetry axis are listed. It is seen in the table that the mass flow rate, $\dot{m}$, should be lower than roughly 0.03 to realize $K_n > 0.1$ with $T_0 = 290$ K where T_0 is the stagnation temperature. The Mach number at the nozzle exit, M_e, is approximately 10 for $\dot{m} = 0.03$ g/s and decreases as the mass flow rate decreases. Therefore, the mass flow rate of $\dot{m} = 0.03$ g/s may be a desired flow rate to realize both $K_n \sim 0.1$ and $M_e \sim 10$, which are favorable for hypersonic rarefied flow applications.

To examine the influence of flow rarefaction, a comparison is made between the numerical results of the nozzle flow obtained by the DSMC method and by the Navier-Stokes equations (CFD). In Fig.4, radial distribution of the pressure, the number density, Mach number, and the streamwise velocity obtained by the DSMC and the CFD method are compared at the nozzle exit for $\dot{m} = 0.03$ g/s. It is seen that the nozzle exit pressure, p_e, is approximately 0.3 Pa in the DSMC result, while p_e is as high as 0.9 Pa in the CFD result at the flow center. The number density is also slightly higher in the CFD result than in the DSMC result at the flow center and in the vicinity of the nozzle surface. The boundary layer development is more critical in the CFD results as the mass flow rate decreases, though the results are not shown here. Note that a non-slip boundary condition is used in the CFD calculations. Due to the excessive boundary layer development, the CFD predicts higher temperature and density than the DSMC. For $\dot{m} = 0.03$ g/s, although the velocity is approximately the same between DSMC and CFD at the flow center, the lower temperature in the DSMC results in the higher Mach number. The core flow diameter increases as $\dot{m}$ increases, and for $\dot{m} = 0.03$ g/s, the core flow diameter is approximately 10 mm, as seen in Fig.4. From the above comparison, even inside the nozzle, the continuum method was found not to predict the flow field correctly.

The flow with the test model was calculated by the DSMC method for $\dot{m} = 0.01$, 0.02, and 0.03 g/s, in order to compare predictions of the model displacement with the experimental results. In this calculation, the test model position is finally determined so that the aerodynamic force acting on the model balances the gravitational force of restitution. Figure 5b shows a comparison between Mach number contours without and with the test model for $\dot{m} = 0.03$ g/s. In this case, the test model is found to rest at a streamwise displacement of 30.57 mm. It is seen that the Mach number decreases significantly ahead of the test model, indicating a merged shock layer, and the influence of

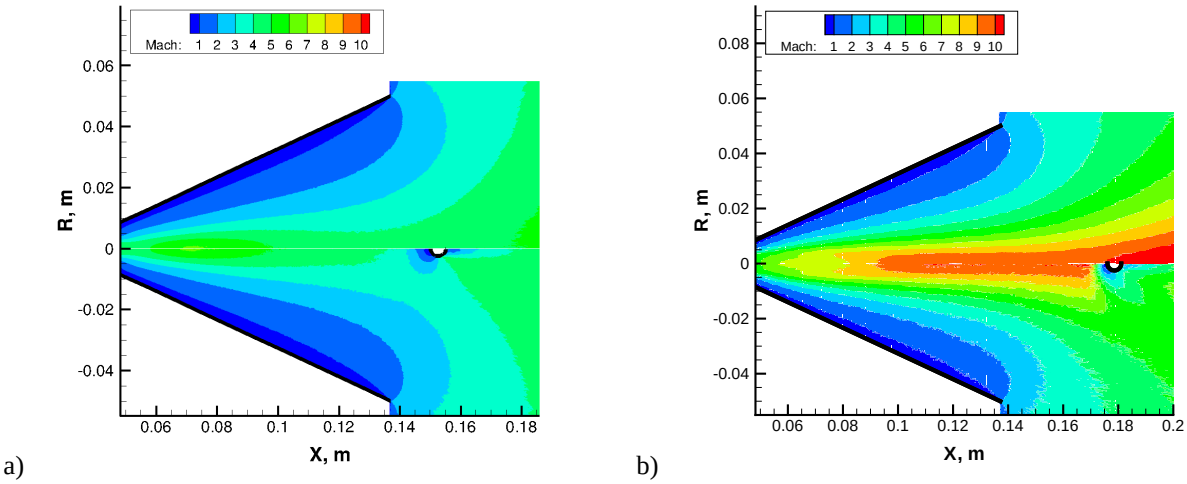

FIGURE 5. Comparison between Mach number contours calculated by DSMC without (upper) and with (lower) test model for a) $\dot{m} = 0.01$ and b) 0.03 g/s.

TABLE 2. Displacement on the symmetry axis for $T_0 = 290$ K

Mass flow $\dot{m}$, g/s	Measured Δx, mm	DSMC (Diffuse, $T_W = 290$ K) Δx, mm	DSMC (Specular) Δx, mm
0.01	4.1±1.0	5.50±0.25	4.43±0.25
0.02	15.6±1.0	17.79±0.25	15.21±0.25
0.03	28±1.0	30.57±0.25	26.29±0.25

the test model extends to approximately 5-mm upstream of the test model. Such a disturbed flow region is wider for the lower mass flow rate. As seen in Fig.5a, the influence of the test model extends to approximately 20-mm upstream of the test model for $\dot{m} = 0.01$ g/s. Because the flow field is significantly influenced by the test model, estimation of the model displacement is very complicated, and the coupled simulations of the test flow with the model motion is necessary to obtain accurate predictions of the model displacement.

In Table 2, the model displacement predicted by the DSMC calculation is compared with that measured in the experiment on the symmetry axis ($z = 0$). In the DSMC calculation, the test model surface was assumed to be diffuse or specular. The wall temperature of the test model, T_W, was assumed to be 290 K. It is seen from the table that the displacement of the test model is appreciably sensitive to the surface condition. The difference between the displacement obtained with the diffuse and the specular model amounts to 5 mm for $\dot{m} = 0.03$ g/s. Contrary to the first intuition, the displacement for the specular condition is smaller than that for the diffuse condition for all the mass flow rates. Flow characteristics in the transitional flow regime are somehow different from those in the free-molecule flow regime. Inspection of the flow field has shown that, because the shock stand-off distance in front of the test model is slightly higher for the specular condition, the number density near the test model is higher for the diffuse condition, resulting in higher pressure on the model surface. For these reasons, the model displacement is higher for the diffuse wall than that for the specular wall. It is noted that good agreement is achieved between the measured and calculated results, and the measured displacement is seen to lie between the specular and diffuse results. For $\dot{m} = 0.01$ g/s, the model displacement is somehow overestimated. Note that the errors in the present measurement are ± 1.0 mm.

In Fig.6, the radial distribution of the calculated model displacement is compared with that measured for $\dot{m} = 0.02$ and 0.03 g/s. In the figure, the DSMC results using the diffuse and the specular wall are presented. The radial profile suggests that the dynamic pressure is the maximum at the flow center, and both the number density and the velocity decrease as z increases. It is pointed out that the calculated results agree well with the measurement. For $\dot{m} = 0.03$ g/s, the measured displacement is seen to lie between the specular and the diffuse results in most radial positions, while agreement between the numerical prediction and the measurement is degraded as the mass flow rate decreases. This is because accuracy in model displacement measurement is at the order of ± 1 mm. The difference between the

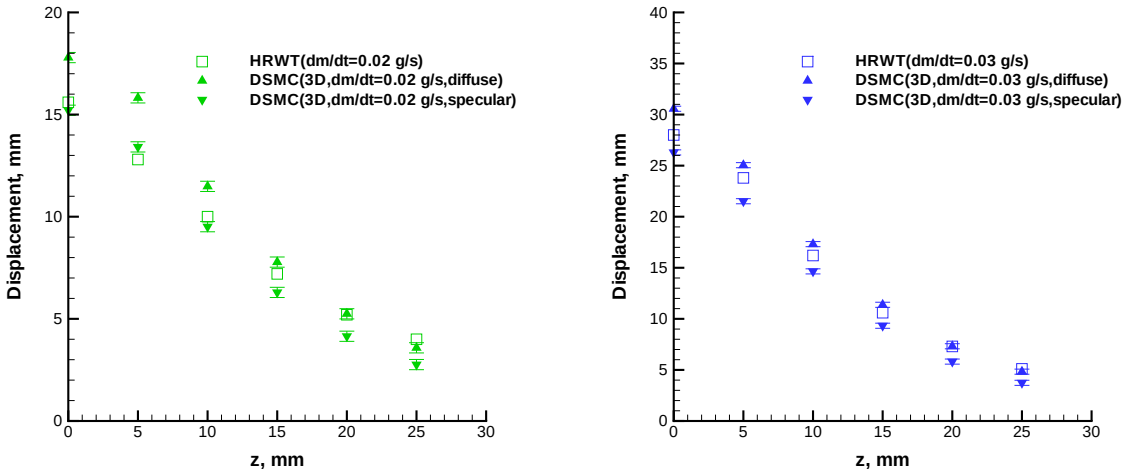

FIGURE 6. Comparisons between measured and calculated displacement of test model for a) $\dot{m} = 0.02$ and b) 0.03 g/s.

specular and the diffuse results is at the order of a few millimeters for $\dot{m} = 0.03$ g/s, which is sufficiently larger than the measurement accuracy. As the mass flow rate decreases, the difference between the two model becomes smaller while errors in model displacement measurement remain unchanged. It is necessary to improve the model displacement measurement accuracy to accomplish more detailed comparison of the numerical results with the experiment. However, the current agreement is satisfactory to estimate the flow properties in the test flow from the computed flow field.

CONCLUSIONS

A pilot model of the hypersonic rarefied wind tunnel has been developed and the flow properties in the test section are investigated both experimentally and numerically. The ambient pressure in the test section was observed to be below 0.3 Pa at the nitrogen flow rate of 0.03 g/s as designed with the preliminary calculations. To probe the test flow, a pendulous sphere model was inserted into the test flow and the model displacement was measured, from which quantitative information about the radial distribution of the dynamic pressure was obtained. Coupled DSMC simulations of the test flow with the test model were successfully conducted to reproduce the radial distribution of the measured model displacement in the streamwise direction. Based on this fact, the two-dimensional distribution of the flow properties is deduced from the computational flow field. It has been shown that the wind tunnel can produce the test flow with the core flow diameter of 10 mm, the Knudsen number of 0.08, and the Mach number of 9.6 at the flow rate of 0.03 g/s.

REFERENCES

1. K. Fujita and A. Noda, AIAA Paper 2009-3606 (2009).
2. K. Fujita, Y. Inatani, and K. Hiraki, *Journal of Spacecraft and Rockets*, **41**(6), 925–931 (2004).
3. J. F. Padilla and I. Boyd, AIAA Paper 2006-3390, (2006).
4. J. Padilla and I. Boyd, *Journal of Thermophysics and Heat Transfer*, **23**(1), 96–105, (2009).
5. J. L. Potter, M. Kinslow, G. D. Arney Jr., and A. B. Bailey, *Progress in Astronautics and Rocketry: Hypersonic Flow Research*, **7**, 599–624, (1962).
6. B. J. Griffith, *Journal of Spacecraft* **4**(7), 919–924, (1967).
7. W. Wuest and G. Koppenwallner, AIAA Paper 68-49, (1968).
8. J. E. Scott, AIAA Paper 1992-3969, (1992).
9. F.C. Hurlbut, AIAA Paper 1992-3971, (1992).
10. E. P. Muntz, I. Boyd, and A. Ketsdever, AIAA Paper 1994-2631, (1994).
11. T. Ozawa, T. Suzuki, K. Fujita, AIAA paper 2010-4513, (2010).